Supporting Information

The differential magnetic relaxation behaviours of the slightly distorted triangular dodecahedral dysprosium analogues in one type of cyano-bridged 3d–4f zig-zag chain compounds

An-Qi Xue,‡[a] Yang-Yu Liu,‡[a] Jia-Xin Li,[b] Yan Zhang,[a] Yin-Shan Meng,[c] Wen-Hua Zhu,*[a] Yi-Quan Zhang,*[b] Hao-Ling Sun,*[d] Fei Wang,[a] Guan-Xia Qiu,[a] Lu-Yu Liang,[a] Xiang Wang[a] and Song Gao*[c]

[a] Hubei Collaborative Innovation Center for Advanced Organic Chemical Materials, Ministry-of-Education Key Laboratory for the Synthesis and Application of Organic Functional Molecules, College of Chemistry and Chemical Engineering, Hubei University, Wuhan 430062, P. R. China.

[b] Jiangsu Key Lab for NSLSCS, School of Physical Science and Technology, Nanjing Normal University, Nanjing, Jiangsu 210023, P. R. China.

[c] Beijing National Laboratory for Molecular Sciences, State Key Laboratory of Rare Earth Materials Chemistry and Applications, College of Chemistry and Molecular Engineering, Peking University, No. 5 Yiheyuan Road, Beijing 100871, P. R. China.

[d] Department of Chemistry and Beijing Key Laboratory of Energy Conversion and Storage Materials, Beijing Normal University, Beijing 100875, P. R. China.

Email: zhuwenhua@pku.org.cn; Email: zhangyiquan@njnu.edu.cn;
Email: gaosong@pku.edu.cn; Email: haolingsun@bnu.edu.cn.

1. Experimental Section

Materials and physical techniques

Unless otherwise stated, all chemicals and solvents were of analytical reagent grade and used as purchased without further purification. All reactions were carried out under aerobic conditions. Elemental analyses of C, H and N were carried out on a Vario Micro Cube elemental analyzer (Elementar Aanlysensysteme GmbH, Germany). IR spectra (4000–400 cm^{-1}) on powered samples were recorded on a Perkin Elmer Spectrum one spectrophotometer using KBr pellets. Powder X-ray diffraction (PXRD) data for the as-prepared samples were collected on a D8 ADVANCE (Bruker AXS, Germany) diffractometer at room temperature using Cu-Kα radiation.

X-ray crystallography

Determination of the unit cell and data collection for complexes **1−3** at 298 K were performed on a Bruker Smart APEX II CCD area detector diffractometer with graphite-monochromated Mo K_α radiation (λ = 0.71073 Å). All of the diffraction data were collected at room temperature and corrected for Lorentz and polarization effects. Adsorption corrections were applied by SADABS method.[1] Using Olex2,[2] the structures were solved by direct methods of SHELXS-97 program and refined by the full-matrix least-squares techniques based on F^2 using SHELXL-2013 program.[3a,b] All of the ordered non-hydrogen atoms were refined with anisotropic thermal parameters. Hydrogen atoms of the coordinated and lattice H_2O molecules were located by difference Fourier map and refined isotropically with constrains for the ideal geometry of H_2O molecules with an O−H distance of 0.96 Å and an H−O−H angle of 105°. Organic hydrogen atoms were introduced on calculated positions and refined with isotropic thermal parameters and a fixed geometry riding on their parent atoms.[3c,d] The crystal data and structural refinement details of **1−3** are respectively summarized in Table 1. The selected bond lengths and angles of **1−3** are listed in Tables S1−S6 in the ESI. CCDC 1982929–1982931.

Magnetic measurement

Static magnetic measurements including temperature-dependent magnetic susceptibility in the range of 2−300 K, and field-dependent magnetization of **1−3** were carried out on a Quantum Design MPMS-XL5 SQUID magnetometer. Alternating current (AC) susceptibilities of **1** (1−1000 Hz) were measured using a Quantum Design MPMS-XL5 SQUID magnetometer. AC susceptibilities of **2** and **3** (100−10000 Hz) were measured using a Quantum Design PPMS magnetometer. All of the magnetic measurements were performed on polycrystalline samples tightly packed with grease and sealed with film to avoid the anisotropic orientation. Diamagnetic corrections were made with Pascal's constants for all the constituent atoms.[4]

2. Structural Data and Diagram

Table S1 Selected bond lengths (Å) and angles (°) for **1**

Y(1)–O(1)	2.261(2)	Y(1)–O(2)	2.396(2)
Y(1)–O(3)	2.371(2)	Y(1)–N(1)	2.498(3)
Fe(1)–C(1)	1.958(3)	Fe(1)–C(2)	1.969(4)
Fe(1)–C(3)	1.962(3)		
O(1)–Y(1)–O(1)#1	151.16(12)	O(2)–Y(1)–O(2)#1	70.79(11)
O(1)–Y(1)–O(2)	69.08(8)	O(2)–Y(1)–O(3)	77.37(9)
O(1)–Y(1)–O(2)#1	139.73(8)	O(2)#1–Y(1)–O(3)	74.24(9)
O(1)–Y(1)–O(3)	93.69(10)	O(3)#1–Y(1)–O(3)	144.99(12)
O(1)–Y(1)–O(3)#1	94.90(10)		
O(1)–Y(1)–N(1)	78.64(9)	O(3)–Y(1)–N(1)	69.20(8)
O(1)–Y(1)–N(1)#1	78.83(9)	O(3)–Y(1)–N(1)#1	145.81(9)
O(2)–Y(1)–N(1)	131.29(9)	N(1)–Y(1)–N(1)#1	76.62(13)
O(2)–Y(1)–N(1)#1	128.27(9)		
C(1)#2–Fe(1)–C(1)	180.0	C(2)#2–Fe(1)–C(2)	180.0
C(1)–Fe(1)–C(2)	89.10(13)	C(3)–Fe(1)–C(2)	90.50(14)
C(1)–Fe(1)–C(2)#2	90.90(13)	C(3)#2–Fe(1)–C(2)	89.51(14)
C(1)–Fe(1)–C(3)	90.83(13)	C(3)–Fe(1)–C(3)#2	180.0
C(1)–Fe(1)–C(3)#2	89.17(13)		
N(1)–C(1)–Fe(1)	175.0(3)	N(3)–C(3)–Fe(1)	175.7(3)
N(2)–C(2)–Fe(1)	177.2(3)	C(1)–N(1)–Y(1)	155.5(2)

Symmetry codes： #1 –x,y, –z+1/2, #2 –x–1/2,–y–1/2,–z.

Table S2 Hydrogen bonding geometry for **1**: lengths (Å) and angles (°)

D–H···A	d(D–H)	d(H···A)	d(D···A)	<(DHA)
O(2)–H(2A)···O(4)	0.94	2.21	2.857(4)	125.7
O(2)–H(2B)···N(2)#3	0.93	1.95	2.823(4)	155.3
O(3)–H(3A)···N(3)#4	0.930(19)	1.84(2)	2.769(4)	172(4)
O(3)–H(3B)···N(3)#2	0.922(18)	2.52(3)	3.364(4)	152(3)
O(4)–H(4B)···N(1)#5	0.96(2)	2.529(17)	3.336(5)	142.2(3)
O(4)–H(4B)···N(1)#4	0.96(2)	2.529(17)	3.336(5)	142.2(3)

Symmetry codes： #1 –x,y,–z+1/2，#2 –x–1/2,–y–1/2,–z，#3 x+1/2,y+1/2,z，#4 x,y+1,z，#5 –x,y+1,–z+1/2.

Table S3 Selected bond lengths (Å) and angles (°) for **2**

Dy(1)–O(1)	2.271(4)	Dy(1)–O(2)	2.417(4)
Dy(1)–O(3)	2.385(4)	Dy(1)–N(1)	2.499(5)
Fe(1)–C(1)	1.938(6)	Fe(1)–C(2)	1.949(6)
Fe(1)–C(3)	1.943(6)		
O(1)–Dy(1)–O(1)#1	151.4(2)	O(2)–Dy(1)–O(2)#1	70.7(2)
O(1)–Dy(1)–O(2)	68.98(14)	O(2)–Dy(1)–O(3)	77.20(15)
O(1)–Dy(1)–O(2)#1	139.57(14)	O(2)#1–Dy(1)–O(3)	74.52(15)
O(1)–Dy(1)–O(3)	93.67(16)	O(3)#1–Dy(1)–O(3)	145.2(2)
O(1)–Dy(1)–O(3)#1	94.80(16)		
O(1)–Dy(1)–N(1)	78.77(15)	O(3)–Dy(1)–N(1)	69.31(14)
O(1)–Dy(1)–N(1)#1	78.84(15)	O(3)–Dy(1)–N(1)#1	145.53(15)
O(2)–Dy(1)–N(1)	131.28(15)	N(1)–Dy(1)–N(1)#1	76.2(2)
O(2)–Dy(1)–N(1)#1	128.59(15)		
C(1)#2–Fe(1)–C(1)	180.0	C(2)#2–Fe(1)–C(2)	180.0
C(1)–Fe(1)–C(2)	90.3(2)	C(3)–Fe(1)–C(2)	91.0(2)
C(1)–Fe(1)–C(2)#2	89.7(2)	C(3)#2–Fe(1)–C(2)	89.0(2)
C(1)–Fe(1)–C(3)	91.3(2)	C(3)–Fe(1)–C(3)#2	180.0
C(1)–Fe(1)–C(3)#2	88.7(2)		
N(1)–C(1)–Fe(1)	176.1(5)	N(3)–C(3)–Fe(1)	176.8(6)
N(2)–C(2)–Fe(1)	178.0(5)	C(1)–N(1)–Dy(1)	154.5(4)

Symmetry codes： #1 –x,y, –z+1/2, #2 –x–1/2,–y–1/2,–z.

Table S4 Hydrogen bonding geometry for **2**: lengths (Å) and angles (°)

D–H···A	d(D–H)	d(H···A)	d(D···A)	<(DHA)
O(2)–H(2B)···O(4)	0.940(19)	1.96(2)	2.856(7)	160(5)
O(2)–H(2A)···N(2)#3	0.941(19)	1.89(2)	2.834(7)	178(6)
O(3)–H(3A)···N(3)#4	0.946(19)	1.84(2)	2.783(6)	172(5)
O(3)–H(3B)···N(3)#2	0.946(19)	2.47(3)	3.365(7)	159(4)
O(4)–H(4B)···N(1)#5	0.96(2)	2.524(17)	3.333(7)	142.3(3)
O(4)–H(4B)···N(1)#4	0.96(2)	2.524(17)	3.333(7)	142.3(3)

Symmetry codes： #1 –x,y,–z+1/2，#2 –x–1/2,–y–1/2,–z，#3 x+1/2,y+1/2,z，#4 x,y+1,z，#5 –x,y+1,–z+1/2.

Table S5 Selected bond lengths (Å) and angles (°) for **3**

Dy(1)–O(1)	2.264(2)	Dy(1)–O(2)	2.407(2)
Dy(1)–O(3)	2.390(2)	Dy(1)–N(1)	2.515(3)
Co(1)–C(1)	1.922(3)	Co(1)–C(2)	1.930(4)
Co(1)–C(3)	1.923(4)		
O(1)–Dy(1)–O(1)#1	150.67(13)	O(2)–Dy(1)–O(2)#1	70.89(13)
O(1)–Dy(1)–O(2)	69.28(9)	O(2)–Dy(1)–O(3)	76.96(9)
O(1)–Dy(1)–O(2)#1	140.03(9)	O(2)#1–Dy(1)–O(3)	74.50(9)
O(1)–Dy(1)–O(3)	93.41(10)	O(3)#1–Dy(1)–O(3)	144.78(13)
O(1)–Dy(1)–O(3)#1	95.37(10)		
O(1)–Dy(1)–N(1)	78.39(10)	O(3)–Dy(1)–N(1)	69.23(9)
O(1)–Dy(1)–N(1)#1	78.72(9)	O(3)–Dy(1)–N(1)#1	145.99(9)
O(2)–Dy(1)–N(1)	131.08(9)	N(1)–Dy(1)–N(1)#1	76.77(13)
O(2)–Dy(1)–N(1)#1	128.32(9)		
C(1)#2–Co(1)–C(1)	180.0	C(2)#2–Co(1)–C(2)	180.0
C(1)–Co(1)–C(2)	89.39(14)	C(3)–Co(1)–C(2)	90.18(15)
C(1)–Co(1)–C(2)#2	90.61(14)	C(3)#2–Co(1)–C(2)	89.82(15)
C(1)–Co(1)–C(3)	90.44(14)	C(3)–Co(1)–C(3)#2	180.0
C(1)–Co(1)–C(3)#2	89.56(14)		
N(1)–C(1)–Co(1)	175.2(3)	N(3)–C(3)–Co(1)	175.4(3)
N(2)–C(2)–Co(1)	177.1(3)	C(1)–N(1)–Dy(1)	155.4(3)

Symmetry codes： #1 –x,y, –z+1/2, #2 –x–1/2,–y–1/2,–z.

Table S6 Hydrogen bonding geometry for **3**: lengths (Å) and angles (°)

D–H···A	d(D–H)	d(H···A)	d(D···A)	<(DHA)
O(2)–H(2B)···O(4)	0.927(18)	2.00(2)	2.840(5)	151(4)
O(2)–H(2A)···N(2)#3	0.941(19)	1.88(2)	2.817(4)	171(4)
O(3)–H(3A)···N(3)#4	0.946(19)	1.84(2)	2.784(4)	175(4)
O(3)–H(3B)···N(3)#2	0.922(18)	2.47(2)	3.344(5)	158(3)
O(4)–H(4B)···N(1)#5	0.973(19)	2.511(16)	3.329(5)	141.5(3)
O(4)–H(4B)···N(1)#4	0.973(19)	2.511(16)	3.329(5)	141.5(3)

Symmetry codes： #1 –x,y,–z+1/2，#2 –x–1/2,–y–1/2,–z，#3 x+1/2,y+1/2,z，#4 x,y+1,z，#5 –x,y+1,–z+1/2.

Table S7 Continuous shape measures (CShM) for **1–3** using SHAPE 2.1

	1	**2**	**3**
OP-8	32.822	32.796	32.775
HPY-8	24.720	24.867	24.700
HBPY-8	16.733	16.774	16.926
CU-8	10.308	10.412	10.186
SAPR-8	2.865	2.886	2.810
TDD-8	0.501	0.495	0.487
JGBF-8	12.560	12.538	12.708
JETBPY-8	30.181	30.113	30.311
JBTPR-8	2.910	2.907	2.883
BTPR-8	2.661	2.652	2.636
JSD-8	2.143	2.115	2.139
TT-8	10.613	10.722	10.489
ETBPY-8	25.240	25.392	25.450

OP-8 = (D_{8h}) Octagon

HPY-8 = (C_{7v}) Heptagonal pyramid

HBPY-8 = (D_{6h}) Hexagonal bipyramid

CU-8 = (O_h) Cube

SAPR-8 = (D_{4d}) Square antiprism

TDD-8 = (D_{2d}) Triangular dodecahedron

JGBF-8 = (D_{2d}) Johnson gyrobifastigium J26

JETBPY-8 = (D_{3h}) Johnson elongated triangular bipyramid J14

JBTPR-8 = (C_{2v}) Biaugmented trigonal prism J50

BTPR-8 = (C_{2v}) Biaugmented trigonal prism

JSD-8 = (D_{2d}) Snub diphenoid J84

TT-8 = (T_d) Triakis tetrahedron

ETBPY-8 = (D_{3h}) Elongated trigonal bipyramid

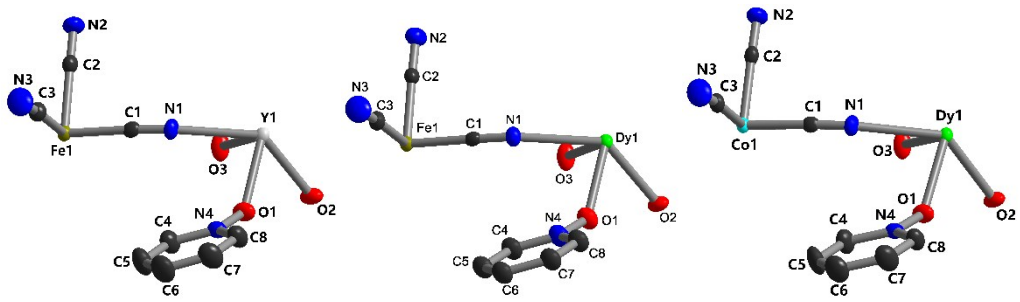

(a) (b) (c)

Fig. S1. The asymmetric units of compounds (a) **1**, (b) **2** and (c) **3** are drawn with thermal ellipsoids (50 % probability)

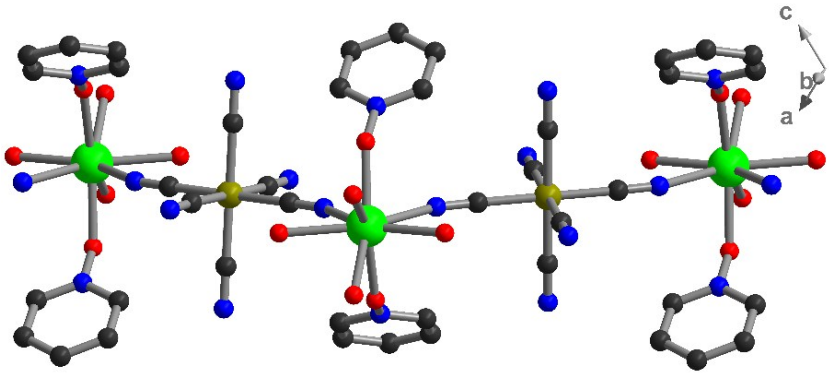

Fig. S2. View of the zig-zag chain structure of compound **2**.

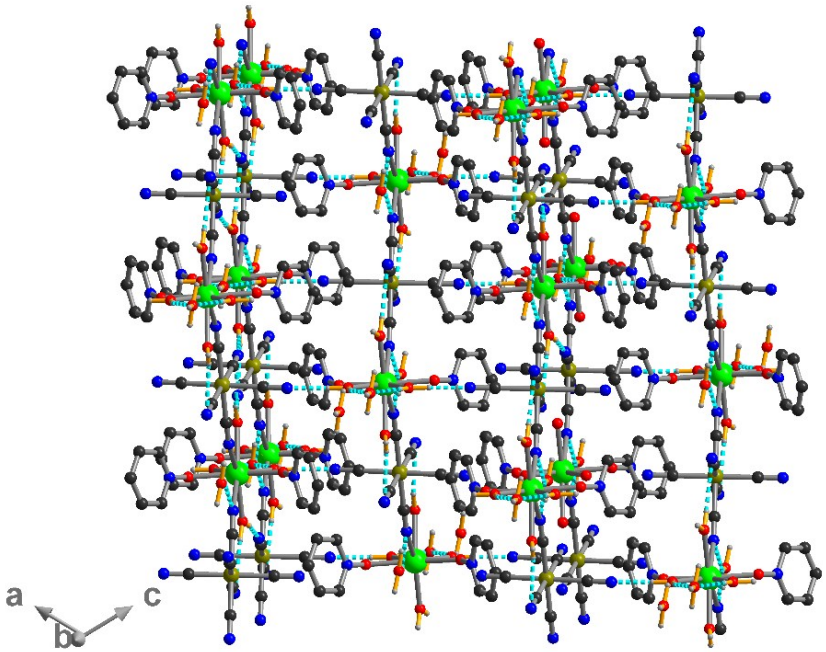

Fig. S3. View of the packing pattern of compound **2** along the *b* direction.

3. Powder XRD Analyses

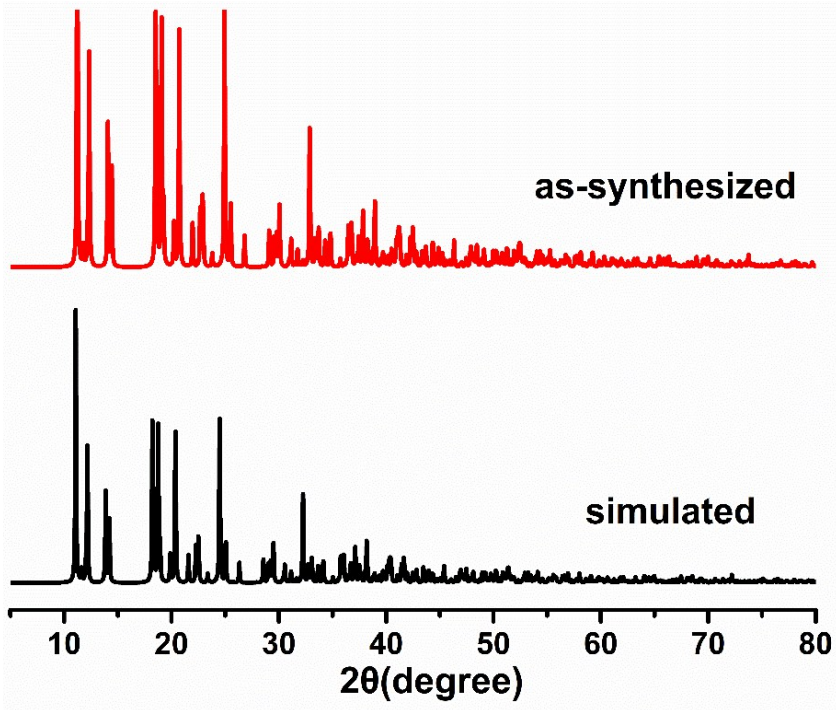

Fig. S4. Powder X-ray diffraction pattern of compound **1** for the as-synthesized sample and the simulated one.

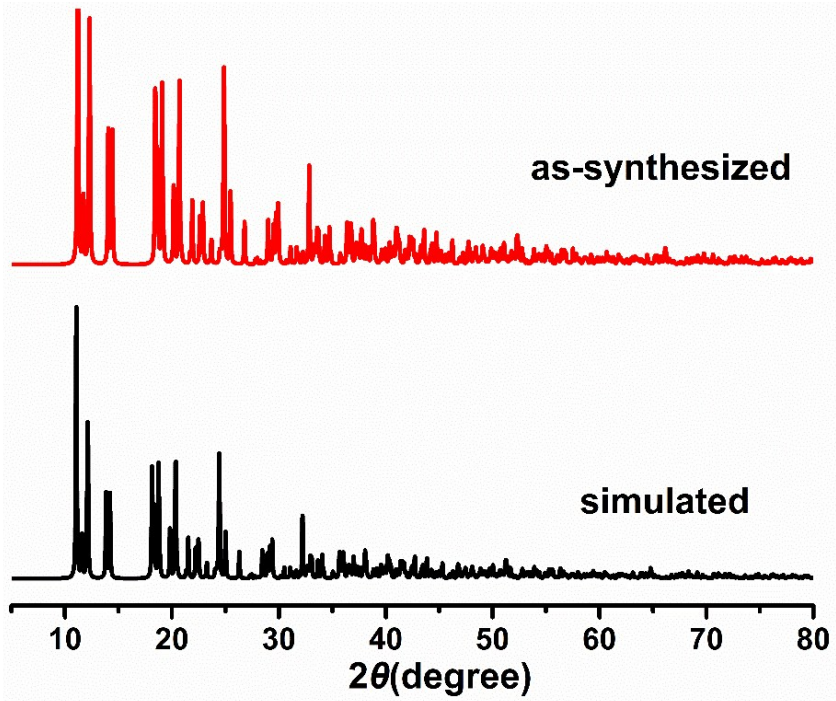

Fig. S5. Powder X-ray diffraction pattern of compound **2** for the as-synthesized sample and the simulated one.

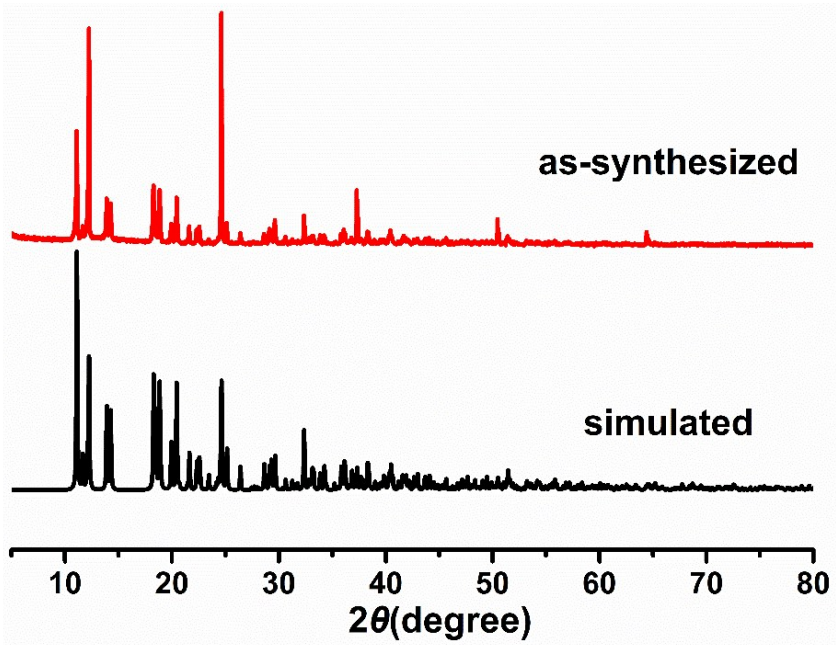

Fig. S6. Powder X-ray diffraction pattern of compound **3** for the as-synthesized sample and the simulated one.

4. Magnetic Properties

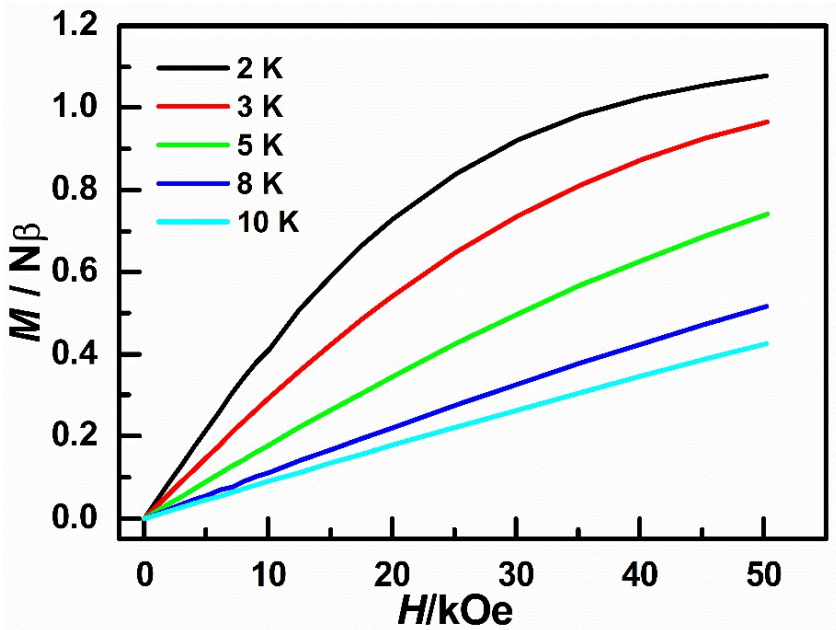

Fig. S7. Field dependence of the magnetization at the temperatures of 2, 3, 5, 8 and 10 K for a polycrystalline sample of **1**.

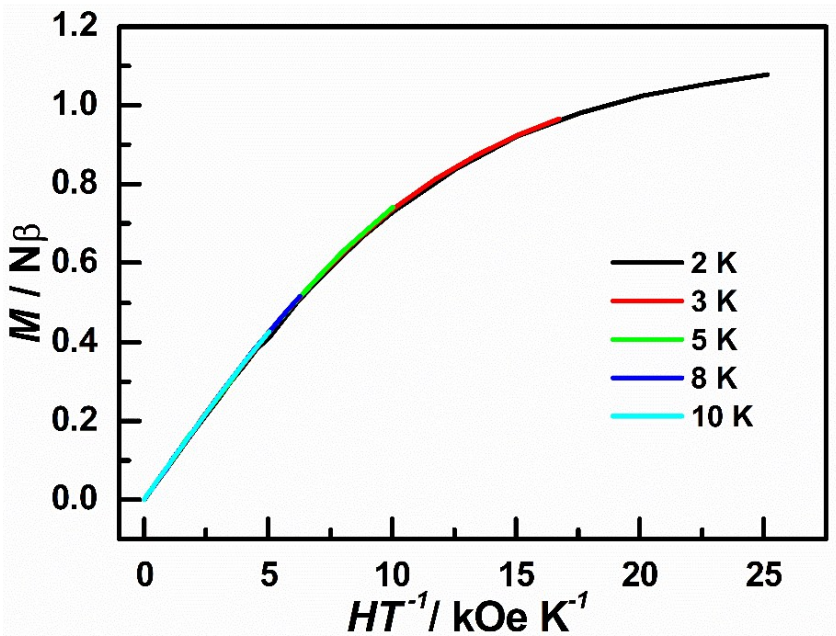

Fig. S8. Plots of the reduced magnetization *M* vs *H*/*T* at the temperatures of 2, 3, 5, 8 and 10 K for a polycrystalline sample of **1**.

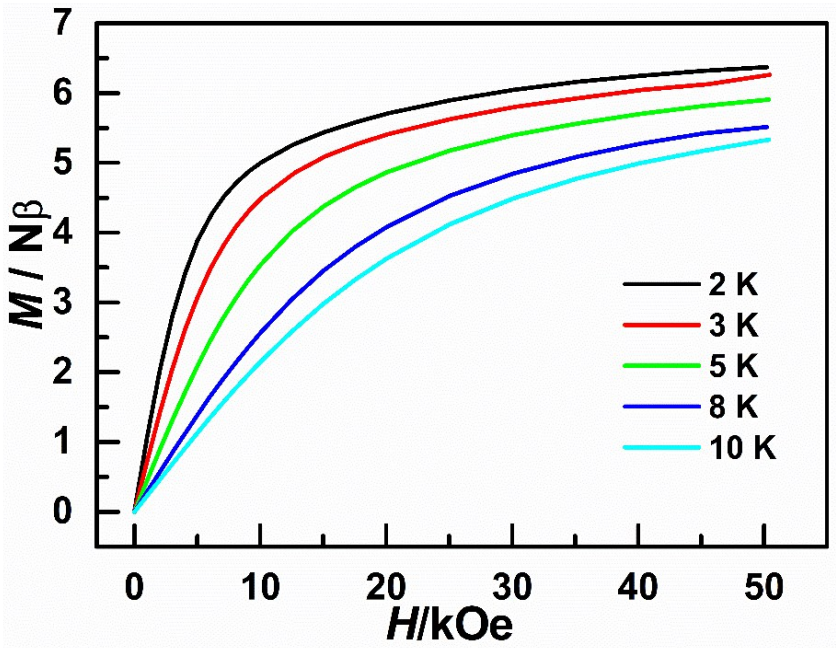

Fig. S9. Field dependence of the magnetization at the temperatures of 2, 3, 5, 8 and 10 K for a polycrystalline sample of **2**.

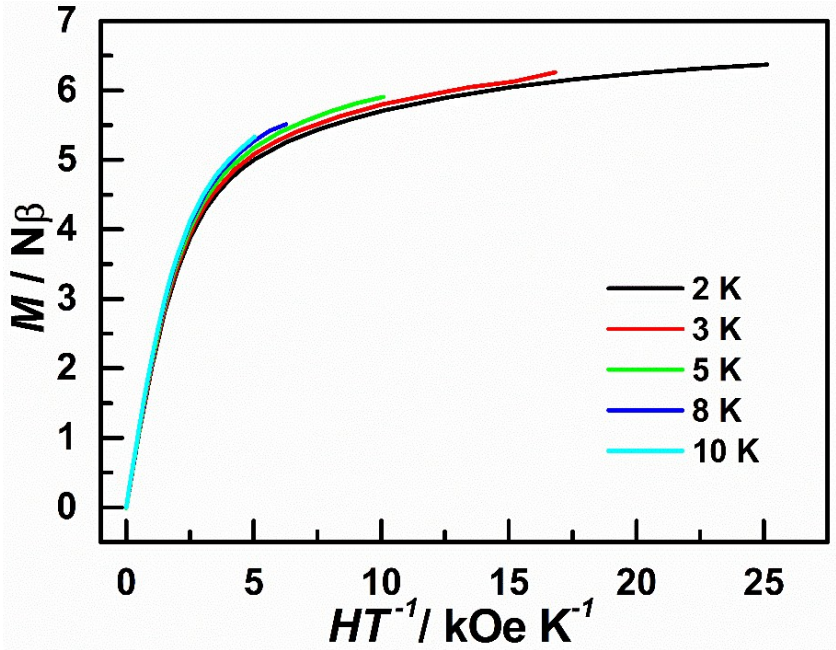

Fig. S10. Field dependence of the magnetization at the temperatures of 2, 3, 5, 8 and 10 K for a polycrystalline sample of **2**.

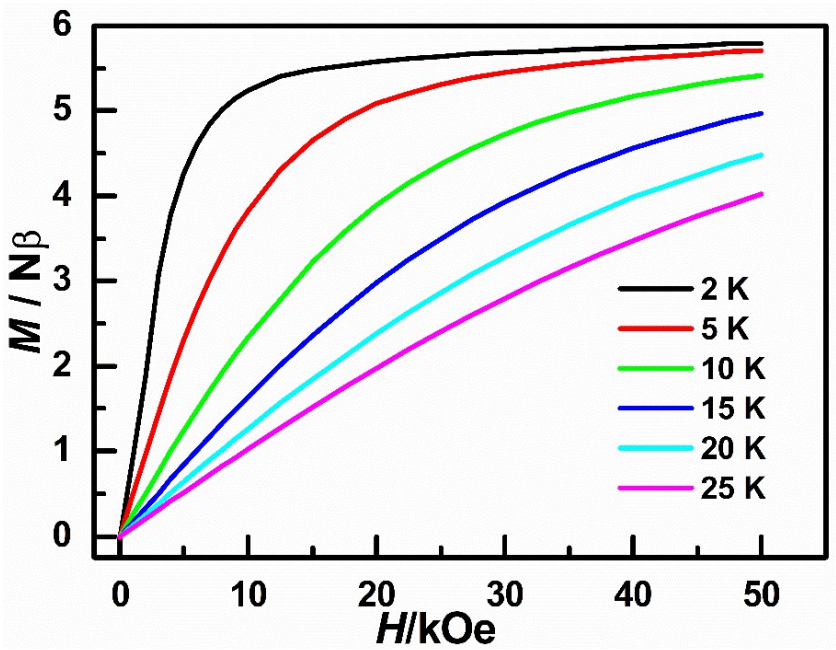

Fig. S11. Field dependence of the magnetization at the temperatures of 2, 5, 10, 15, 20 and 25 K for a polycrystalline sample of **3**.

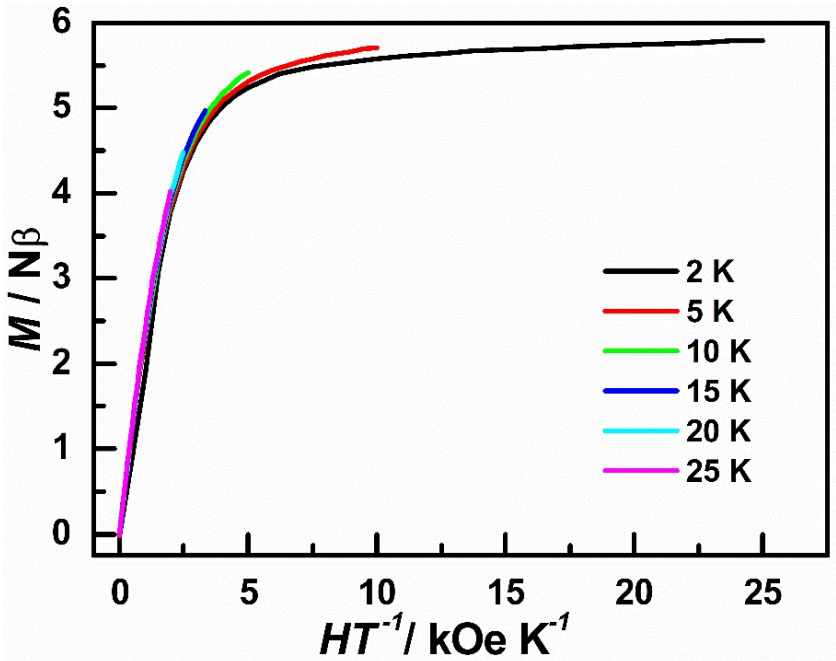

Fig. S12. Field dependence of the magnetization at the temperatures of 2, 5, 10, 15, 20 and 25 K for a polycrystalline sample of **3**.

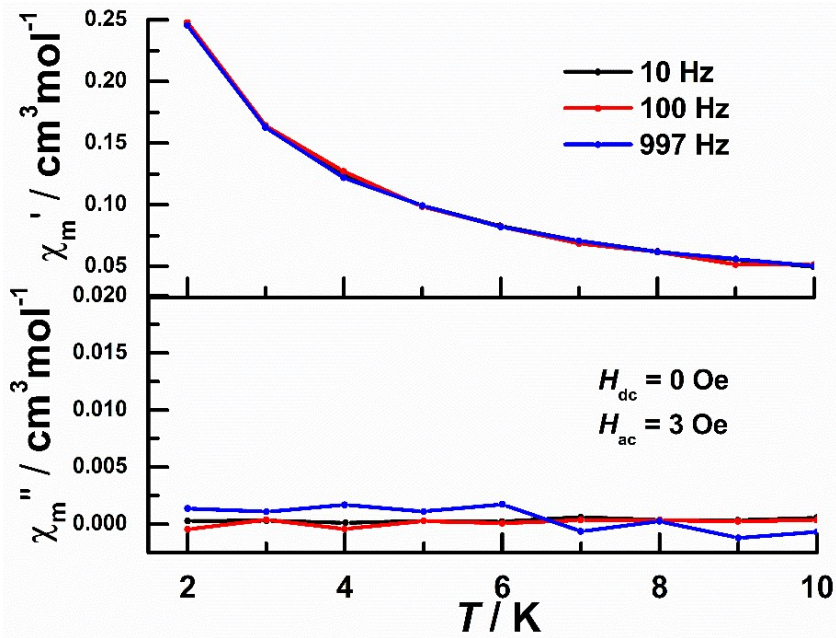

Fig. S13. Temperature dependence of the χ' and χ'' ac susceptibility components for compound **1** under zero dc field at indicated ac frequencies.

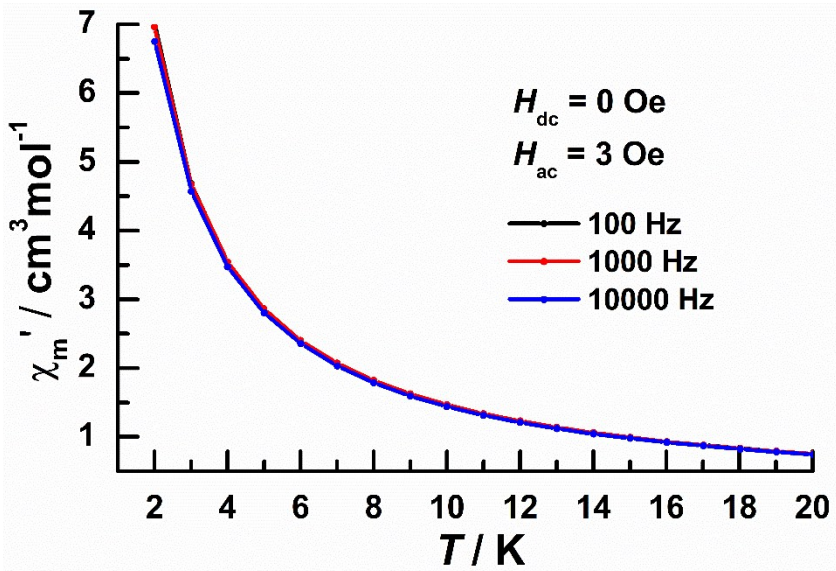

Fig. S14. Temperature dependence of the χ' ac susceptibility components for **2** under zero dc field at indicated ac frequencies.

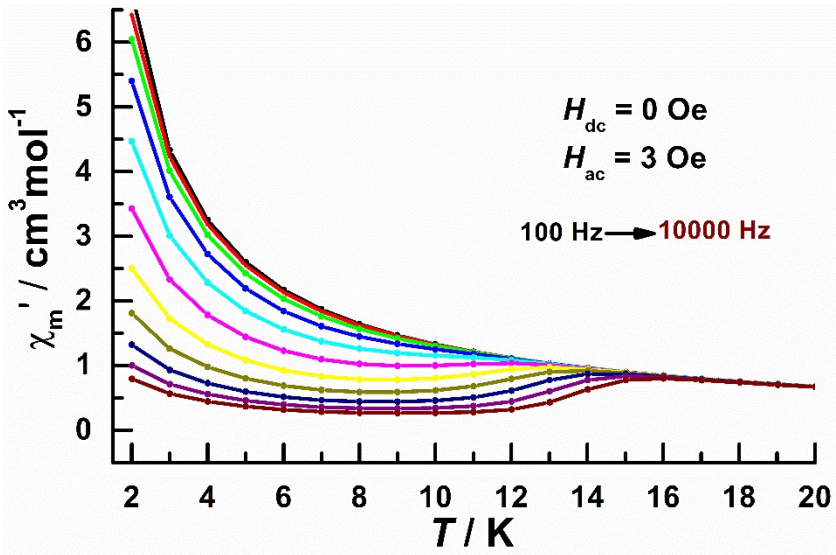

Fig. S15. Temperature dependence of the χ' ac susceptibility components for **3** under zero dc field at indicated ac frequencies.

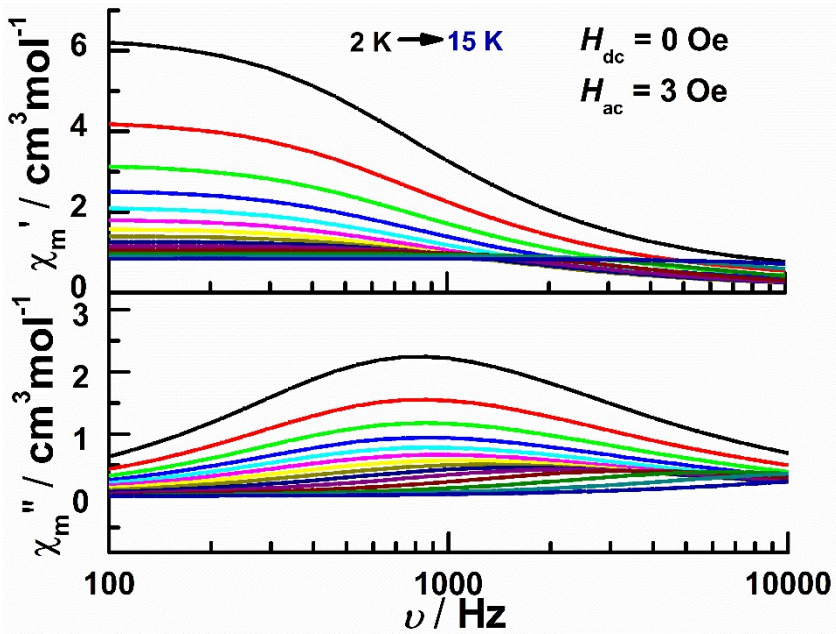

Fig. S16. Frequency dependence of the χ' and χ'' ac susceptibility components for compound **3** under zero dc field at indicated temperature.

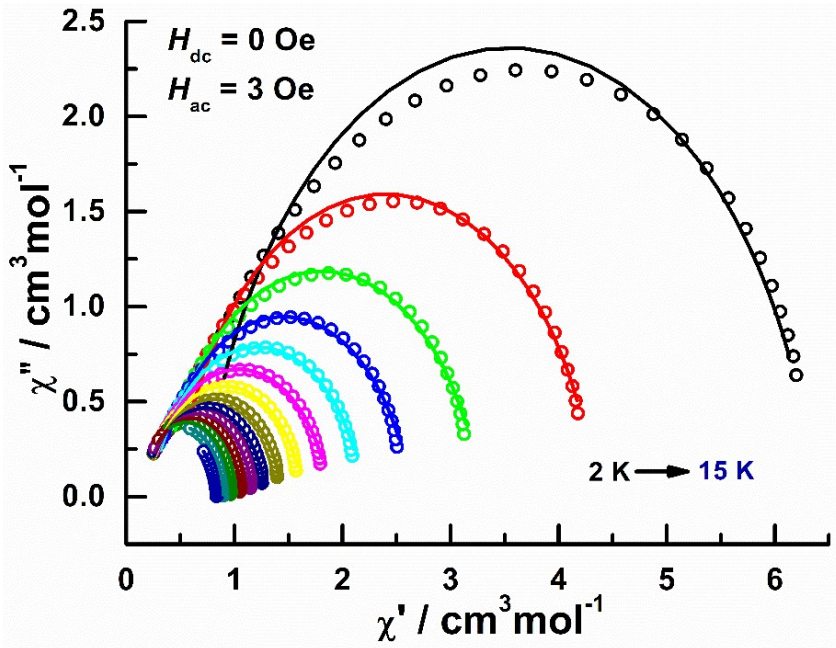

Fig. S17. The Cole–Cole plots in the range of 2–15 K (1 K as a step) for compound **3** under zero dc field. The solid lines are the least-square fitting of the data to a distribution of single relaxation processes with the generalized Debye model.

Table S8 Relaxation parameters from the best fitting of the Cole–Cole diagrams in the range of 2–15 K by the generalized Debye model under zero dc field for **3**.

T(K)	χ_S(cm^3 mol^{-1})	χ_T(cm^3 mol^{-1})	τ(s)	α
2.0	0.72	0.64E+1	0.18E-3	0.114
3.0	0.46	0.43E+1	0.17E-3	0.127
4.0	0.33	0.33E+1	0.17E-3	0.138
5.0	0.27	0.26E+1	0.17E-3	0.141
6.0	0.23	0.22E+1	0.16E-3	0.143
7.0	0.20	0.19E+1	0.15E-3	0.144
8.0	0.18	0.16E+1	0.14E-3	0.143
9.0	0.17	0.14E+1	0.11E-3	0.136
10.0	0.17	0.13E+1	0.90E-4	0.120
11.0	0.16	0.12E+1	0.66E-4	0.093
12.0	0.16	0.11E+1	0.43E-4	0.059
13.0	0.14	0.97	0.25E-4	0.035
14.0	0.13	0.90	0.13E-4	0.033
15.0	0.12	0.84	0.63E-5	0.065

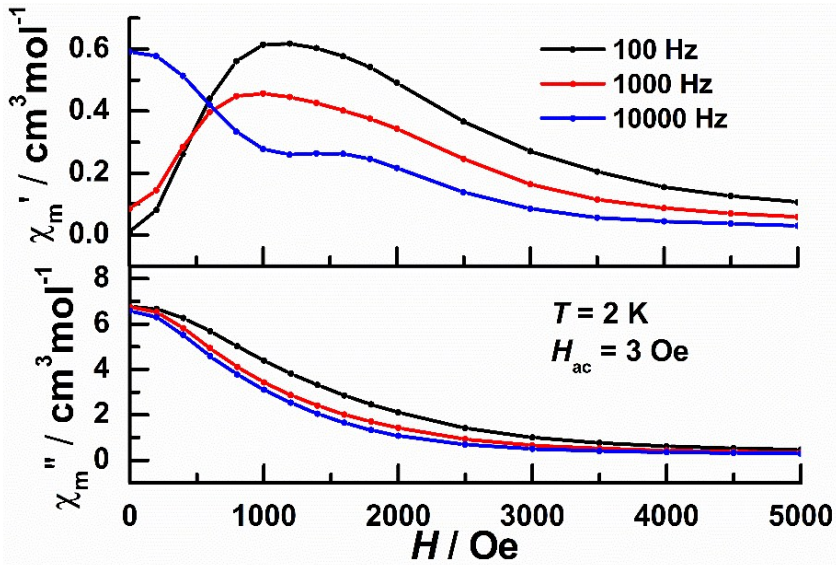

Fig. S18. Field dependence of the χ' and χ'' ac susceptibilities components for **2** with f = 100, 1000 and 10000 Hz.

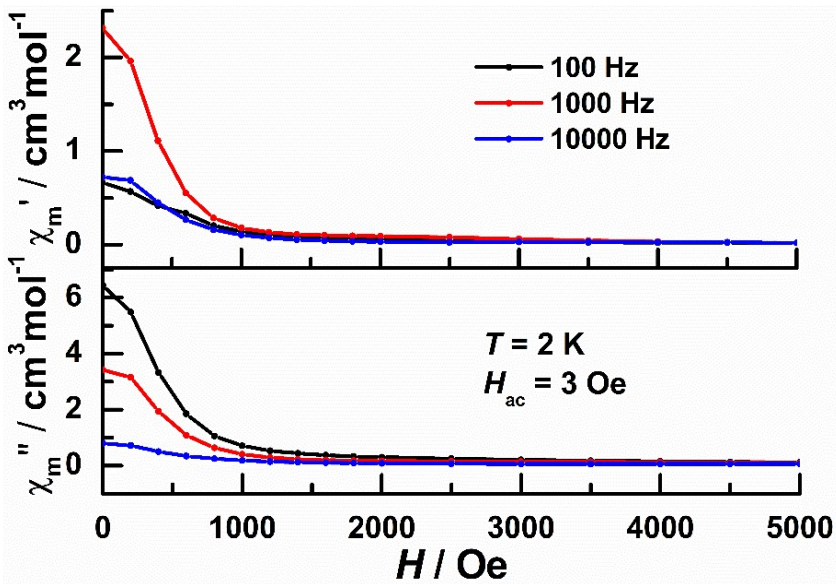

Fig. S19. Field dependence of the χ' and χ'' ac susceptibilities components for **3** with f = 100, 1000 and 10000 Hz.

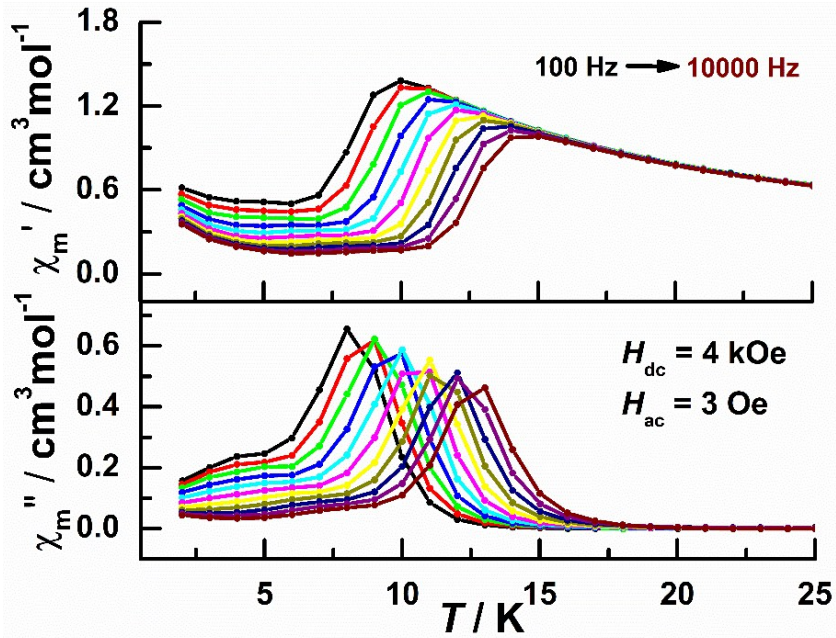

Fig. S20. Temperature dependence of the χ' and χ'' ac susceptibility components for **2** under a 4 kOe dc field at indicated ac frequencies.

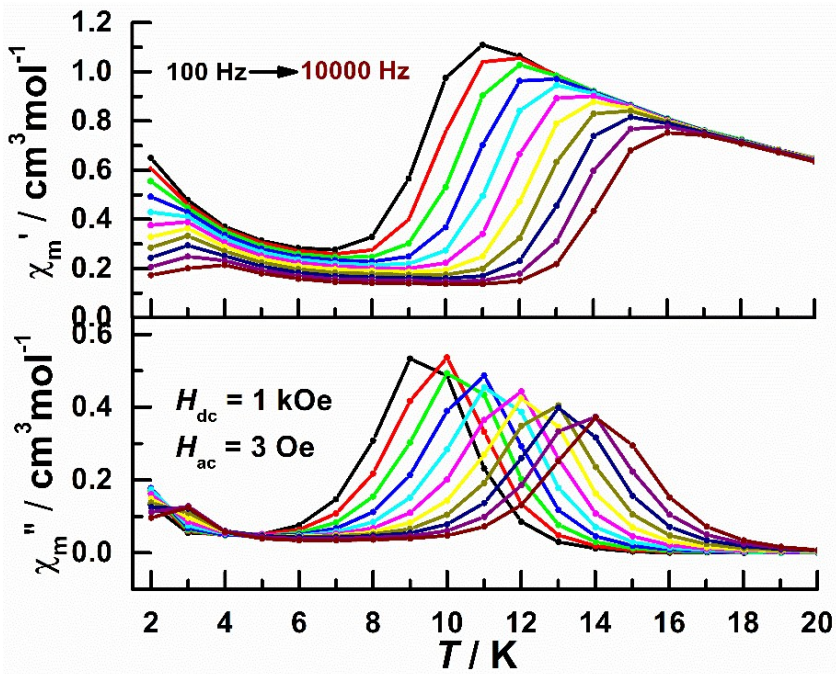

Fig. S21. Temperature dependence of the χ' and χ'' ac susceptibility components for **3** under a 1 kOe dc field at indicated ac frequencies.

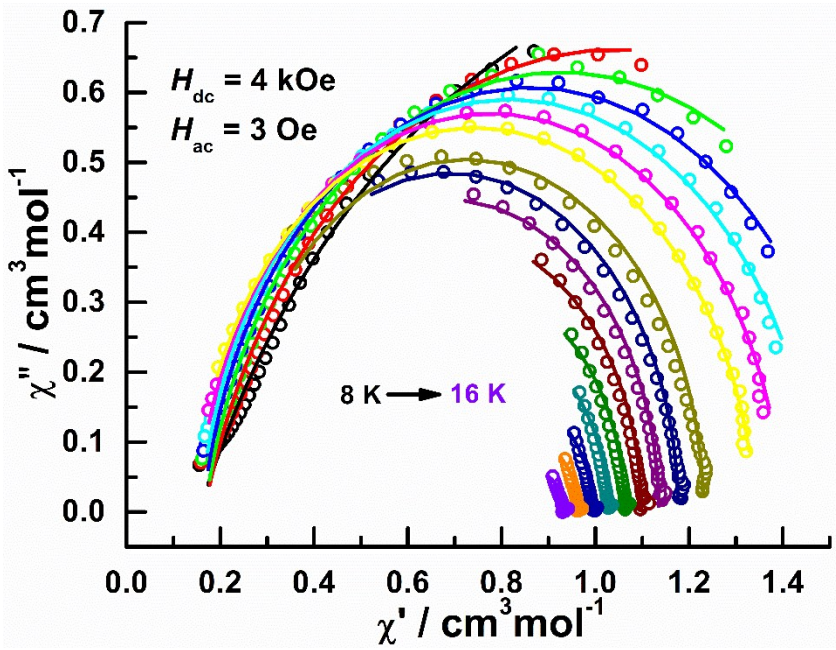

Fig. S22. The Cole–Cole plots in the range of 8–16 K (0.5 K as a step) for **2** under a 4 kOe dc field. The solid lines are the least-square fitting of the data to a distribution of single relaxation processes with the generalized Debye model.

Table S9 Relaxation parameters from the best fitting of the Cole–Cole diagrams in the range of 8–16 K by the generalized Debye model under a 4 kOe dc field for **2**.

T(K)	χ_S(cm^3 mol^{-1})	χ_T(cm^3 mol^{-1})	τ(s)	α
8.0	0.15	2.58	0.41E-2	0.013
8.5	0.17	1.91	0.15E-2	0.012
9.0	0.17	1.69	0.82E-3	0.010
9.5	0.16	1.56	0.48E-3	0.007
10.0	0.16	1.48	0.29E-3	0.004
10.5	0.15	1.40	0.17E-3	0.002
11.0	0.14	1.34	0.10E-3	0.001
12.0	0.22	1.23	0.40E-4	0.014
12.5	0.21	1.18	0.23E-4	0.005
13.0	0.24	1.14	0.15E-4	0.004
13.5	0.31	1.10	0.10E-4	0.003
14.0	0.42	1.06	0.79E-5	0.002
14.5	0.53	1.03	0.66E-5	0.001
15.0	0.68	0.99	0.70E-5	0.001
15.5	0.76	0.96	0.76E-5	0.001
16.0	0.82	0.93	0.10E-4	0.001

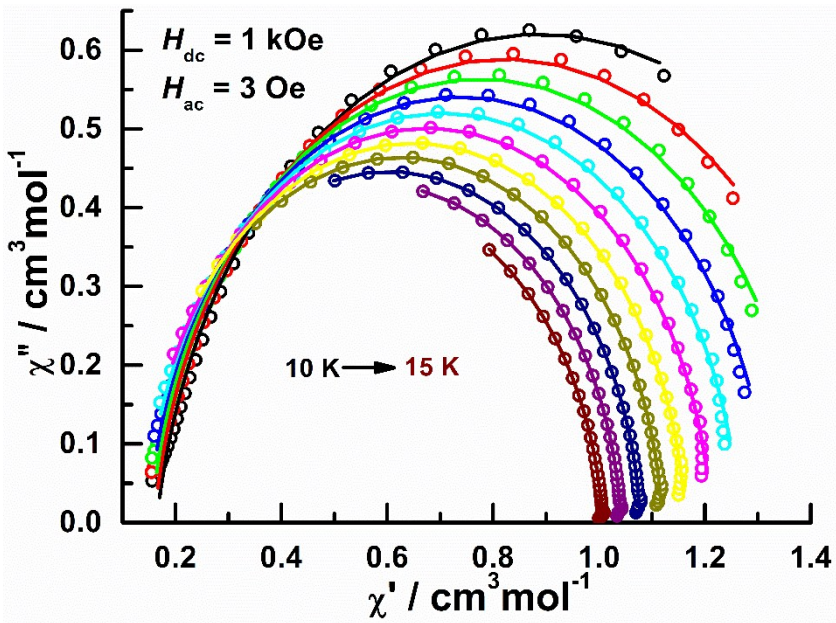

Fig. S23. The Cole–Cole plots in the range of 10–15 K (0.5 K as a step) for **3** under a 1 kOe dc field. The solid lines are the least-square fitting of the data to a distribution of single relaxation processes with the generalized Debye model.

Table S10 Relaxation parameters from the best fitting of the Cole–Cole diagrams in the range of 10–15 K by the generalized Debye model under a 1 kOe dc field for **3**.

T(K)	χ_S(cm^3 mol^{-1})	χ_T(cm^3 mol^{-1})	τ(s)	α
10.0	0.16	1.61	0.10E-2	0.006
10.5	0.16	1.48	0.61E-3	0.005
11.0	0.15	1.40	0.37E-3	0.002
11.5	0.15	1.33	0.23E-3	0.002
12.0	0.14	1.27	0.14E-3	0.001
12.5	0.14	1.21	0.84E-4	0.000
13.0	0.14	1.16	0.52E-4	0.000
13.5	0.13	1.12	0.32E-4	0.000
14.0	0.13	1.08	0.20E-4	0.000
14.5	0.12	1.04	0.13E-4	0.000
15.0	0.10	1.01	0.81E-5	0.000

5. Ab initio calculations

Complexes **2** and **3** are both one-dimensional chains including only one type of Dy^{III} ion, thus we only need to calculate one Dy^{III} fragment for each of them. (see Figure S24 for the calculated model structures of Dy^{III} fragments in complexes **2** and **3**) on the basis of single-crystal X-ray determined geometry have been carried out by complete-active-space self-consistent field (CASSCF) with MOLCAS 8.4[5] program package. During the calculation of the individual Dy^{III} fragments for **2** and **3**, the influence of the nearest neighboring Dy^{III} ions were taken into account by the closed-shell La^{III} ab initio embedding model potentials (AIMP; La.ECP.deGraaf.0s.0s.0e-La-(LaMnO3.).

The basis sets for all atoms are atomic natural orbitals from the MOLCAS ANO-RCC library: ANO-RCC-VTZP for Dy^{III}; VTZ for close O and N; VDZ for distant atoms. The calculations employed the second order Douglas-Kroll-Hess Hamiltonian, where scalar relativistic contractions were taken into account in the basis set and the spin-orbit couplings were handled separately in the restricted active space state interaction (RASSI-SO) procedure. For individual Dy^{III} fragment, active electrons in 7 active spaces include all *f* electrons (CAS(9 in 7 for Dy^{III})) in the CASSCF calculation. To exclude all the doubts, we calculated all the roots in the active space. We have mixed the maximum number of spin-free state which was possible with our hardware (all from 21 sextets, 128 from 224 quadruplets, 130 from 490 doublets for Dy^{III}). SINGLE_ANISO[6-8] program was used to obtain the energy levels, ***g*** tensors, predominant m_J values, magnetic axes, *et al.,* based on the above CASSCF/RASSI-SO calculations.

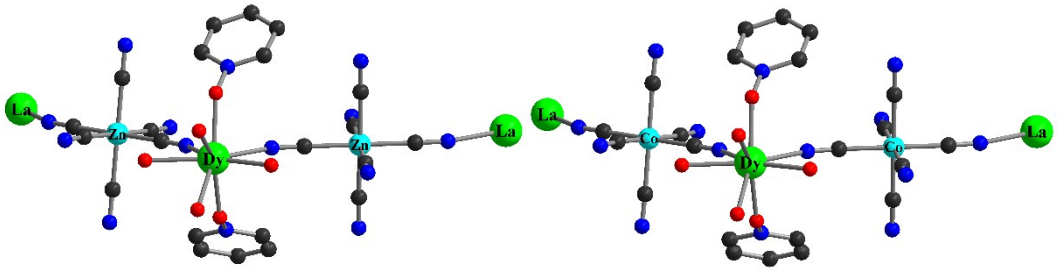

Fig. S24. Calculated model structures of individual Dy^{III} fragments in (a) complexes **2** and (b) **3**; H atoms are omitted.

Table S11. Calculated energy levels (cm^{-1}), ***g*** (g_x, g_y, g_z) tensors and predominant m_J values of the lowest eight Kramers doublets (KDs) of individual Dy^{III} fragments for complexes **2** and **3** using CASSCF/ RASSI-SO with MOLCAS 8.4.

KDs	**2**				**3**			
	E/cm^{-1}	***g***		m_J	E/cm^{-1}	***g***		m_J
1	0.0	g_x	0.012	±15/2	0.0	g_x	0.001	±15/2
		g_y	0.021			g_y	0.002	
		g_z	19.420			g_z	19.594	
2	106.6	g_x	1.892	±7/2	151.7	g_x	0.341	±13/2
		g_y	4.038			g_y	0.397	
		g_z	14.900			g_z	16.116	
3	132.7	g_x	1.904	±9/2	228.0	g_x	3.668	±7/2
		g_y	4.207			g_y	5.715	
		g_z	9.856			g_z	10.973	
4	190.3	g_x	4.885	±5/2	262.2	g_x	7.809	±5/2
		g_y	6.408			g_y	6.076	
		g_z	9.960			g_z	1.986	
5	224.0	g_x	0.186	±13/2	301.8	g_x	2.441	±11/2
		g_y	0.296			g_y	2.854	
		g_z	19.155			g_z	11.326	
6	247.3	g_x	0.357	±1/2	319.2	g_x	7.314	±3/2
		g_y	1.524			g_y	7.021	
		g_z	15.688			g_z	1.907	
7	263.8	g_x	0.340	±11/2	332.6	g_x	1.030	±1/2
		g_y	1.056			g_y	4.020	
		g_z	15.958			g_z	11.939	
8	280.4	g_x	0.205	±3/2	341.6	g_x	0.319	±9/2
		g_y	2.495			g_y	4.058	
		g_z	17.316			g_z	14.718	

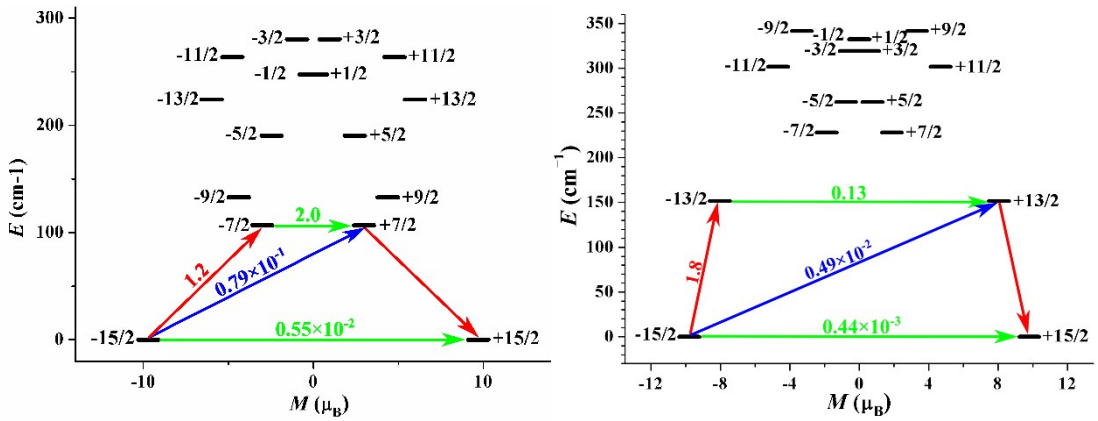

Fig. S25. Magnetization blocking barriers of individual Dy^{III} fragments in complexes **2** (left) and **3** (right). The thick black lines represent the KDs of the individual Dy^{III} fragments as a function of their magnetic moment along the magnetic axis. The green lines correspond to diagonal matrix element of the transversal magnetic moment; the blue line represent Orbach relaxation processes. The path shown by the red arrows represents the most probable path for magnetic relaxation in the corresponding compounds. The numbers at each arrow stand for the mean absolute value of the corresponding matrix element of transition magnetic moment.

6. References

1 G. M. Sheldrick, *SADABS*, *Program for Siemens area detector absorption correction*, University of Göttingen, 1996.

2 O. V. Dolomanov, L. J. Bourhis, R. J. Gildea, J. A. K. Howard and H. J. Puschmann, *Appl. Crystallogr.*, 2009, **42**, 339−341.

3 (*a*) G. M. Sheldrick, *SHELXS97*, *Program for the solution of crystal structures*, University of Göttingen, Germany, 1997; (*b*) G. M. Sheldrick, *Acta Crystallogr.*, *Sect. A: Fundam. Crystallogr.*, 2008, **A64**, 112−122; (*c*) T. Shiga, M. Ohba and H. Okawa, *Inorg. Chem. Commun.*, 2003, **6**, 15−18; (*d*) S. Akine, T. Matsumoto, T. Taniguchi and T. Nabeshima, *Inorg. Chem.*, 2005, **44**, 3270−3274.

4 O. Kahn, *Molecular Magnetism*, Wiley-VCH, New York, 1993.

5 F. Aquilante, J. Autschbach, R. K. Carlson, L. F. Chibotaru, M. G. Delcey, L. De Vico, I. Fdez Galvan, N. Ferre, L. M. Frutos, L. Gagliardi, M. Garavelli, A. Giussani, C. E. Hoyer, G. Li Manni, H. Lischka, D. Ma, P. A. Malmqvist, T. Muller, A. Nenov, M. Olivucci, T. B. Pedersen, D. Peng, F. Plasser, B. Pritchard, M. Reiher, I. Rivalta, I. Schapiro, J. Segarra-Marti, M. Stenrup, D. G. Truhlar, L. Ungur, A. Valentini, S. Vancoillie, V. Veryazov, V. P. Vysotskiy, O. Weingart, F. Zapata and R. Lindh, *J. Comput. Chem.*, 2016, **37**, 506-541.

6 L. Ungur and L. F. Chibotaru, *Chem. Eur. J.*, 2017, **23**, 3708−3718.

7 L. F. Chibotaru, L. Ungur, C. Aronica, H. Elmoll, G. Pilet and D. Luneau. *J. Am. Chem. Soc.*, 2008, **130**, 12445−12455.

8 L. Ungur, W. Van den Heuvel and L. F. Chibotaru, *New J. Chem.*, 2009, **33**, 1224−1230.